Electrochimica Acta 353 (2020) 136530

Contents lists available at ScienceDirect

Electrochimica Acta

journal homepage: www.elsevier.com/locate/electacta

Air-breathing cathode self-powered supercapacitive microbial fuel cell with human urine as electrolyte

Carlo Santoro [a, 1, *], Xavier Alexis Walter [a], Francesca Soavi [b], John Greenman [a, c], Ioannis Ieropoulos [a, **]

[a] Bristol BioEnergy Centre, Bristol Robotics Laboratory, T-Block, UWE, Coldharbour Lane, Bristol BS16 1QY, UK
[b] Department of Chemistry "Giacomo Ciamician", Alma Mater Studiorum – Università; di Bologna, Via Selmi, 2, 40126, Bologna, Italy
[c] Biological, Biomedical and Analytical Sciences, UWE, Coldharbour Lane, Bristol, BS16 1QY, UK

ARTICLE INFO

Article history:
Received 6 February 2020
Received in revised form
5 May 2020
Accepted 25 May 2020
Available online 29 May 2020

Keywords:
Microbial fuel cell
Supercapacitive mode
Human urine
Galvanostatic discharges
Current/power pulses

ABSTRACT

In this work, a membraneless microbial fuel cell (MFC) with an empty volume of 1.5 mL, fed continuously with hydrolysed urine, was tested in supercapacitive mode (SC-MFC). In order to enhance the power output, a double strategy was used: i) a double cathode was added leading to a decrease in the equivalent series resistance (ESR); ii) the apparent capacitance was boosted up by adding capacitive features on the anode electrode. Galvanostatic (GLV) discharges were performed at different discharge currents. The results showed that both strategies were successful obtaining a maximum power output of 1.59 ± 0.01 mW (1.06 ± 0.01 mW mL^{-1}) at pulse time of 0.01 s and 0.57 ± 0.01 mW (0.38 ± 0.01 mW mL^{-1}) at pulse time of 2 s. The highest energy delivered at i_{pulse} equal to 2 mA was 3.3 ± 0.1 mJ. The best performing SC-MFCs were then connected in series and parallel and tested through GLV discharges. As the power output was similar, the connection in parallel allowed to roughly doubling the current produced. Durability tests over ≈5.6 days showed certain stability despite a light overall decrease.

1. Introduction

Bioelectrochemical systems (BES) are capturing more and more the consideration of the scientific community worldwide for their unique characteristics of transforming the organic compounds into electricity and/or other value-added products (VAPs) [1–5]. Among BESs, microbial fuel cells (MFCs) are of interest because they can remove organics and pollutants from a waste stream and generate simultaneously useful electricity for practical applications [2–5]. Microbial fuel cells have shown the possibilities of degrading the diverse organic compounds varying from single substrate to more complex and variegated wastewaters [6,7]. The fact that MFCs produce rather than consume electricity during their operations makes the technology to be suitable for substituting traditional aerobic wastewater treatment [2–5]. Moreover, since MFCs produce directly electricity through the chemical energy stored in the organic compounds bonds and not indirectly, MFCs can play as competitors to the anaerobic digester technologies in which biogas is created and then transformed to electricity, therefore electricity is produced only indirectly [2–5]. MFCs hold a great potential in the field of wastewater treatment, but are currently limited in terms of industrial scalability, capital expenditure and to a lesser extent, universal applicability (e.g. where there is only solid matter), constraints which have nevertheless been faced by almost all other technologies during their critical development phase.

In order to enter into the market and substitute the existing technologies, MFCs have to: i) reduce the overall cost; ii) increase the cathode reaction rate; iii) improve the power that can be delivered. As MFCs are a low power producing technology, reducing the overall cost is very important. This means that both anode and cathode materials and eventually the membrane/separator have to be durable, reliable and cheap [8–13]. Different anode materials have been investigated with the intention of increasing the biotic/abiotic interphase and therefore enhance the electron transfer from the bacteria to the electrode [14,15]. Among the materials

* Corresponding author.
** Corresponding author.
E-mail addresses: carlo.santoro830@gmail.com (C. Santoro), ioannis.ieropoulos@brl.ac.uk (I. Ieropoulos).
[1] Currently: Department of Chemical Engineering and Analytical Science, The University of Manchester, The Mill, Sackville Street, M13AL Manchester, UK.

https://doi.org/10.1016/j.electacta.2020.136530

Abbreviations

AC	activated carbon
BES	Bioelectrochemical system
C_A	anodic apparent capacitance
C_C	cathodic apparent capacitance
C_{cell}	apparent capacitance
E_{pulse}	pulse energy
ESR	equivalent series resistance
GLV	Galvanostatic
i_{pulse}	current pulse
MFC	Microbial Fuel Cell
SC-MFC	Supercapacitive Microbial Fuel Cell
OCP	Open Circuit Potential
OCV	Open Circuit Voltage
ORR	oxygen reduction reaction
PGM-free	platinum group metals-free
P_{max}	maximum power
P_{pulse}	pulse power
PTFE	polytetrafluoroethylene
R_A	anodic ohmic resistance
R_C	cathodic ohmic resistance
SC-MFC-C	Supercapacitive Microbial Fuel Cell with single cathode
SC-MFC-2C	Supercapacitive Microbial Fuel Cell with double cathode
SC-MFC-2CCA	Supercapacitive Microbial Fuel Cell with double cathode and capacitive anode
t_{pulse}	pulse time
VAP	value-added product
$\Delta V_{capacitive,cell}$	voltage variation due to capacitive features
V_{max}	maximum voltage after ohmic drop
$V_{max\ OC}$	voltage at open circuit potential
$\Delta V_{ohmic,cell}$	vertical voltage drop due to the ohmic losses

investigated, carbonaceous materials are the most promising [8,9]. Carbon cloth, paper, veil, brush and felt, plain or modified materials have been successfully investigated in MFCs [16–22]. Recently also metallic based materials have been investigated [23–25]. Stainless steel seems to be promising and for large scale applications also cheaper compared to carbonaceous materials [26,27]. Other metals have also been investigated and molybdenum has shown to be a metal increasing the anodic output [28]. Concerning the cathode, substitution of platinum with cheaper and more durable materials is needed [29–31]. The cathode reaction of reducing oxygen is limited by the circum(neutral) electrolyte operating conditions that do not provide high concentration of reactants (e.g. H^+) [32–34]. Much attention has been devoted to enhance and optimize the oxygen reduction reaction (ORR). As mentioned above, platinum cannot be taken into account due to the high cost and low durability in the presence of anions [35,36] and therefore alternatives have been proposed for accelerating ORR. Carbonaceous materials are suitable to be used as cathode catalysts in bioelectrochemical systems [37,38]. Among them, diverse materials such as carbon black, carbon nanotubes, carbon nanofibers, graphene and activated carbon have been investigated [39–44]. The main characteristics of these catalysts for being successful are: i) high surface area and high content in nitrogen defects on the carbonaceous matrix for enhancing the ORR; ii) high electrical conductivity for enhancing electron transfer; iii) high resistivity to corrosion in polluted and harsh environments. Recently, also platinum group metals-free (PGM-free) catalysts were found to be very active towards ORR in (circum)neutral electrolyte. PGM-free materials are catalysts containing an earth abundant transition metal such as Fe, Co, Mn or Ni [45–47]. High performing PGM-free can be categorized into two main groups; the first one that use catalysts produced through pyrolysis (high temperature treatment in controlled atmosphere) of a nitrogen-rich organic precursor and a metal-containing salt [48–52] and the second one through deposition or impregnation of organic molecules with the metal incorporated into their structure such as porphyrins or phthalocyanines [53–56]. Generally, it was previously found that iron was the most active and efficient [57].

Low power output characterize bioelectrochemical systems that operate in neutral pHs and take advantage of slow biological processes. Therefore, the power management has to be optimised in order to harvest successfully the power/current produced [58–60]. Diverse practical applications have also been implemented starting from robotics with GastroBot [61] and the EcoBot family [62–64]. In order to boost the output of MFCs, the latters are usually coupled with a power management system that contains electronics and supercapacitors or batteries [60]. Lately, the capacitive features of the electrodes have been exploited in supercapacitive bioelectrochemical systems and particularly supercapacitive microbial fuel cell (SC-MFC) [65–71]. Capacitive anodes and cathodes have been extensively investigated in the past 5–10 years [72–79]. Particularly, the electrodes of the BESs were utilized as the electrode of an internal supercapacitor and discharged galvanostatically, like a supercapacitor [80]. High current/power pulses were obtained and the electrodes were self-recharged to the initial voltage value conditions due to the red-ox reactions (oxidation of organics and reduction of oxygen) occurring on the two electrodes [80]. Diverse supercapacitive MFCs were tested in different scale varying from 0.5 mL [81] to 1 L [82,83] in different design configurations. These previous design adopted also diverse fuels operating as the electrolyte of the internal supercapacitor. Human urine as fuel was firstly introduced in 2012 [84] and captured the attention of the scientists worldwide in the past few years due to its unique characteristics and properties that make it suitable to be used widely for BESs [85]. Particularly, human urine is of extreme interests due to the high solution conductivity, which help to decrease the ohmic resistance of the electrolyte [86,87].

In this work, a small-size air-breathing cathode membraneless MFC design is presented and investigated in supercapacitive mode. SC-MFC operated in flow with hydrolysed human urine as fuel and electrolyte. Characteristics parameters such as equivalent series resistance (ESR) and apparent capacitance are measured on the overall SC-MFC and on the single electrode. Once the control SC-MFC was characterized, further improvements have been followed in order to decrease the overall ESR and enhance the apparent capacitance. Moreover, the SC-MFCs were connected in series and parallel and the electrochemical output was investigated. Durability tests of 4000 cycles of discharge and self-recharge were carried out in order to establish the variation in performance, ESR and apparent capacitance over time.

2. Materials and method

2.1. Microbial fuel cell construction and materials

The SC-MFCs had a cubical shape and was built using Plexiglas pieces that were put together through screws. The cubical had two lateral holes where the cathodes were placed. In the case of the

control SC-MFCs, only one cathode was used and the other lateral hole was closed with a laser cut of the shape of the hole. The empty volume was 2 mL but the displacement volume (containing the anode) was 1.5 mL. Two additional holes were built for the inlet and outlet of the electrolyte through the anodic chamber. At last, a hole was made on the top of the SC-MFCs in order to accommodate the reference electrode to be inserted in the chamber. An image of the operating SC-MFC is reported in Fig. 1.

The anode was built using carbon veil. Particularly, a foil of 2 × 5 cm (10 cm^2) was wrapped into a small cubical shape. The cathode was made with a mixture of activated carbon (AC, 800 $m^2\ g^{-1}$, SK1 P75, CPL Carbon Link, UK) and polytetrafluoroethylene (PTFE) (60% emulsion, Sigma Aldrich) in a ratio in weight of 8 to 2 [88,89]. The mixture was then pressed over a stainless steel mesh using a pin roll. Four layers of PTFE were coated also on the external face (facing atmosphere) of the stainless steel as shown before applying a temperature treatment. The external PTFE diffusion layer was used in order to avoid electrolyte leakage. The SC-MFCs control (in duplicate) named as SC-MFC-C had the anode dimension and composition as described before and one cathode with a geometric surface area of 2.25 cm^2. The second configuration used was named SC-MFC-2C (in duplicate) and differed from the first configuration by the addition of a second cathode on the opposite side of the MFC. The anode was the same size as the first configuration but the cathode geometric area doubled to 4.5 cm^2. In the third configuration, a thin layer composed by activated carbon and PTFE was prepared separately and embedded into the anode electrode. The third configuration named as SC-MFC-2CCA (in duplicate) also had two cathodes electrodes with a total geometric area of 4.5 cm^2. The conditions tested are summarized in Table 1. Experiments were run in duplicates for each condition and the two SC-MFCs were named as A and B. SC-MFCs were firstly individually tested and then the two SC-MFC-2CCAs were studied after being connected in series and in parallel.

2.2. Operating conditions

The MFCs (in duplicate for each studied condition) were inoculated initially with an electrolyte mixture containing 50% in volume of hydrolysed urine and 50% of effluent from well-established and working MFCs fed with hydrolysed urine. The MFCs were connected to an external resistor that was decreased from 5000 Ω to 2500 Ω, 1000 Ω and finally 500 Ω. Once the voltage output was stable, fresh fully hydrolysed urine was used as feedstock. All the SC-MFCs were run in continuous and constant flow of 0.06 mL min^{-1}. The urine used had a pH of 9.1 ± 0.1 and a solution conductivity that varied in the range of 26.2 and 30.3 mS cm^{-1}. Once the voltage was stable, galvanostatic discharges were done on the MFCs singularly considering anode as negative electrode and cathode as positive electrode of an internal supercapacitor. Once these tests were done, SC-MFC-2CCAs were connected firstly in parallel and then in series and galvanostatic discharges were performed.

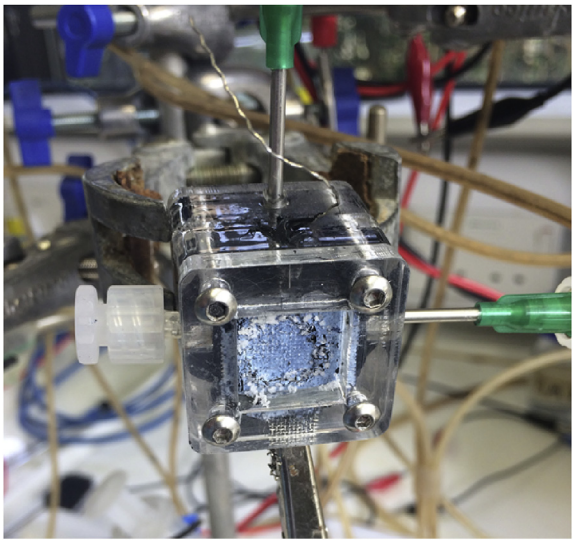

Fig. 1. Image of the SC-MFC used in this study.

2.3. Electrochemical operations

Complete galvanostatic (GLV) discharges were done at different current pulses ($\mathbf{i_{pulse}}$). Experiments were done in duplicates. The MFCs were initially left in open circuit conditions for at least 1 h. After 1 h, the voltage of the MFC was stable at a value named as $\mathbf{V_{max,OC}}$. When the GLV started, a vertical drop in the voltage can be noted. The vertical voltage drop corresponded to the ohmic losses ($\mathbf{\Delta V_{ohmic,cell}}$) of the system and the MFC reach then a value named $\mathbf{V_{max}}$, which is actually the maximum voltage that the MFC can feature. $\mathbf{V_{max}}$ can be described by eq. (1):

$$V_{max} = V_{max,OC} - \Delta V_{ohmic,cell} \quad (1)$$

The ohmic losses named also equivalent series resistance (**ESR**) corresponded to the sum of anode electrode ohmic losses, electrolyte ohmic losses and cathode ohmic losses. ESR can be calculated using eq. (2) as the ratio between $\mathbf{\Delta V_{ohmic,cell}}$ and $\mathbf{i_{pulse}}$:

$$ESR = \frac{\Delta V_{ohmic,cell}}{i_{pulse}} \quad (2)$$

During GLVs, a reference electrode was inserted into the MFC close to the anode electrode. This allowed measuring the anode and cathode potential profile separately. Particularly, also the anode and cathode ohmic resistance named as $\mathbf{R_A}$ and $\mathbf{R_C}$ respectively, can be calculated. Eq. (3) is used for calculating $\mathbf{R_A}$:

$$R_A = \frac{\Delta V_{ohmic,anode}}{i_{pulse}} \quad (3)$$

Eq. (4) instead is used for calculating $\mathbf{R_C}$:

$$R_C = \frac{\Delta V_{ohmic,cathode}}{i_{pulse}} \quad (4)$$

After reaching V_{max}, the voltage continues to decrease and this is due to the electrodes capacitive features. This voltage variation named as capacitive variation ($\mathbf{\Delta V_{capacitive,cell}}$) is used for calculating the capacitance of the cell ($\mathbf{C_{cell}}$) following eq. (5):

$$C_{cell} = \frac{i_{pulse}}{\frac{dV}{dt}} = \frac{i_{pulse}}{s} \quad (5)$$

The slope s is defined as the variation of voltage over time. As done for ESR, also the apparent capacitance can be calculated for anode (C_A) and cathode (C_C) electrode respectively. In the case of C_A and C_C, the variation of the potential during the discharge will be considered. C_A and C_C were calculated according to eq. (6) and eq. (7):

$$C_A = \frac{i_{pulse}}{\frac{dV_{anode}}{dt}} \quad (6)$$

Table 1
Anode and cathode composition of the three conditions tested.

condition	anode	cathode	acronym
control	carbon veil	1 cathode (2.25 cm^2)	SC-MFC-C
double cathode	carbon veil	2 cathodes (4.5 cm^2)	SC-MFC-2C
double cathode & capacitive anode	carbon veil & AC/PTFE	2 cathodes (4.5 cm^2)	SC-MFC-2CCA

$$C_C = \frac{i_{pulse}}{\frac{dV_{cathode}}{dt}} \quad (7)$$

Apparent $\mathbf{C_A}$, $\mathbf{C_C}$ and $\mathbf{C_{cell}}$ can be correlated as shown in eq. (8):

$$C_{cell} = \left(\frac{1}{C_A} + \frac{1}{C_C}\right)^{-1} \quad (8)$$

In the calculation of the apparent capacitance, only the initial linear variation of the cell voltage and electrodes potential is considered. For low i_{pulse}, the cell voltage and electrodes potential reach a plateau that cannot be accounted for the electrostatic double layer but it can be accounted for by the redox reaction occurring at the interface of the electrodes/electrolyte. Electrostatic and faradaic contributions during galvanostatic discharges were deeply studied in a recent investigation [90].

Power and energy are other parameters that are used for characterizing the system. Particularly, the maximum power ($\mathbf{P_{max}}$) achievable by the system is determined using eq. (9):

$$P_{max} = V_{max} \times i_{pulse} \quad (9)$$

$\mathbf{P_{max}}$ considers the ohmic losses of the system but disregard the capacitive losses. The pulse power ($\mathbf{P_{pulse}}$) delivered in a specific time ($\mathbf{t_{pulse}}$) instead is calculated in eq. (10):

$$P_{pulse} = \frac{i_{pulse}\int_0^t V dt}{t_{pulse}} \quad (10)$$

The energy of the pulse is also calculated considering $\mathbf{P_{pulse}}$ and $\mathbf{t_{pulse}}$ as shown in eq. (11):

$$E_{pulse} = P_{pulse} \times t_{pulse} \quad (11)$$

The power is also expressed in function of the volume (mW mL^{-1}) of the MFC that was 1.5 mL.

3. Results and discussion

3.1. Complete discharges of air-breathing cathode supercapacitive MFC

Complete GLVs were achieved on the SC-MFCs at different i_{pulse} varying from 0.5 mA to 5 mA. SC-MFC voltage trends and cathode and anode potential behaviours were presented in Fig. 2.a, Fig. 2.b and Fig. 2.c respectively. $V_{max,OC}$ was measured to be 650 ± 6 mV and was the difference between the cathode potential contribution (47 ± 2 mV vs Ag/AgCl) and the anode potential contribution (−603 ± 5 mV vs Ag/AgCl). The maximum voltage of an MFC operating with organics and using oxygen as final electron acceptor is ≈ 1100 mV [91], therefore the overpotentials can be quantified in ≈450 mV. At pH 9, organic oxidation involving NADH/NAD^+ has a potential of ≈ -600 mV vs Ag/AgCl and this value is close to the anodic potential recorded indicating negligible overpotentials. The overall overpotentials can be attributed exclusively to the cathode.

ESR was evaluated to be 87.9 ± 3.2 Ω and the 20% of it was due to the anode (18.1 ± 0.5 Ω) and the remaining 80% due to the cathode (70.1 ± 2.9 Ω). Larger cathode resistance was also measured in previous works underlying the limitation of this particular electrode [92,93]. The time of complete discharges decreased with the increase in i_{pulse}. Particularly, t_{pulse} of 5.55 ± 0.13 s, 1.54 ± 0.04 s, 0.47 ± 0.02 s, 0.17 ± 0.02 s, 0.07 ± 0.01 s and 0.03 ± 0.01 s were measured for i_{pulse} of 0.5 mA, 1 mA, 2 mA, 3 mA, 4 mA and 5 mA respectively. The apparent capacitance of the SC-MFC and anode and cathode separately can be found in Table S1. Apparent C_{cell} decreased with the current applied indicating a probable contribution from the red-ox reactions occurring on the electrode and therefore a faradaic component. Except for the highest i_{pulse} tested, the apparent capacitance of the cathode was much higher compared to the one of the anode. This can be expected since carbon veil does not exhibit high surface area and does not possess capacitive features. At the contrary, the cathode is composed by AC, which has high surface area and good capacitive features.

3.2. Effect of cathode doubling on the galvanostatic discharges

As the cathode of SC-MFC-Cs showed high R_C contributing to over 80% of the overall ESR, the first action done for improving the performance was to reduce R_C. In order to achieve that, the cathode area was doubled and particularly at both side of the structure, a cathode was inserted. Overall voltage trends and cathode and anode potential behaviors of SC-MFC-2C during GLV discharges were presented in Fig. 3.a, Fig. 3.b and Fig. 3.c, respectively.

This configuration lead to a decrease in cell OCV to 536 ± 6 mV that was ≈114 mV lower compared to the one recorded for SC-MFC-C that was 650 ± 6 mV. In order to understand the cause of this decrease, also the anode and cathode potential were examined. The cathode potential measured similarly as SC-MFC-C (+55 ± 7 mV vs Ag/AgCl), instead the anode had much higher potential. In fact, the anode potential measured −480 ± 3 mV vs Ag/AgCl with a decrease of roughly 120 mV compared to the control. This increase in the anode potential might be due to the addition of the second cathode and therefore the anode resulted to be more exposed to oxygen penetrating through the cathode and negatively affecting the anaerobic environment. Despite this negative aspect, during GLV discharges, showed a significant decrease in R_C and consequently ESR. ESR was measured as 40.0 ± 2.0 Ω with R_A being 16.7 ± 0.5 Ω and RC being 22.2 ± 1.7 Ω. R_A was similar as before while R_C was a third than SC-MFC-C thus indicating that this strategy was advantageous. Despite lower OCV, the SC-MFC-2Cs could be completely discharged at higher i_{pulse} (up to 7 mA). At i_{pulse} of 0.5 mA, t_{pulse} was 8.84 ± 0.59 s, which was almost double compared to SC-MFC-C. At i_{pulse} of 1 mA, t_{pulse} was 2.20 ± 0.05 s. In this case, the t_{pulse} was lower compared to SC-MFC-C considering the same i_{pulse}. Therefore the advantage of lower ESR was only notable at lower i_{pulse}, at higher i_{pulse} instead this advancement disappeared. The overall apparent capacitance of the SC-MFC-2C as well as the anode and the cathode separately are presented in Table S2. Despite lower t_{pulse}, the lower OCV and ESR allowed for a higher apparent capacitance. Apparent cathode capacitance was higher compared to anode capacitance. As the cathode doubled in size, the apparent capacitance of the cathode was always higher at every i_{pulse} investigated.

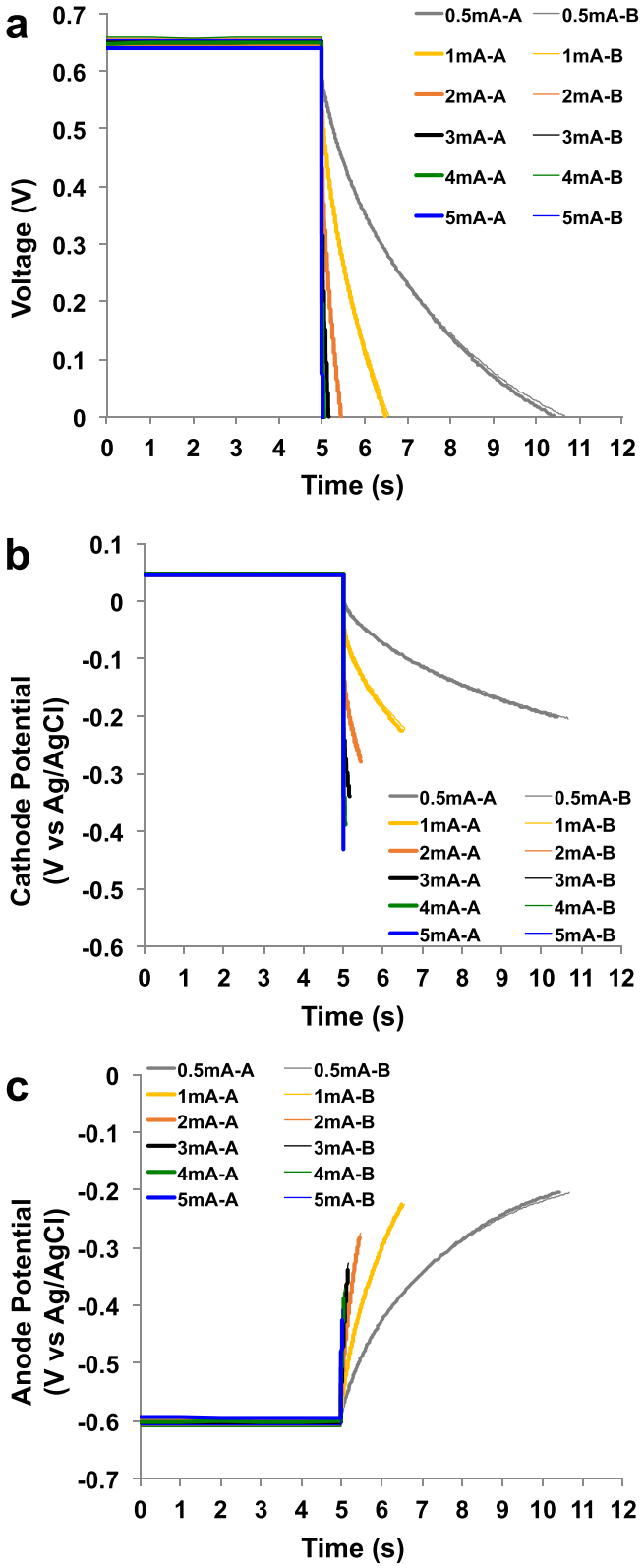

Fig. 2. Complete discharges for SC-MFC at different i_{pulse}. Overall (a), cathode (b), anode (c) profile during the discharge. A and B are the two separate SC-MFCs.

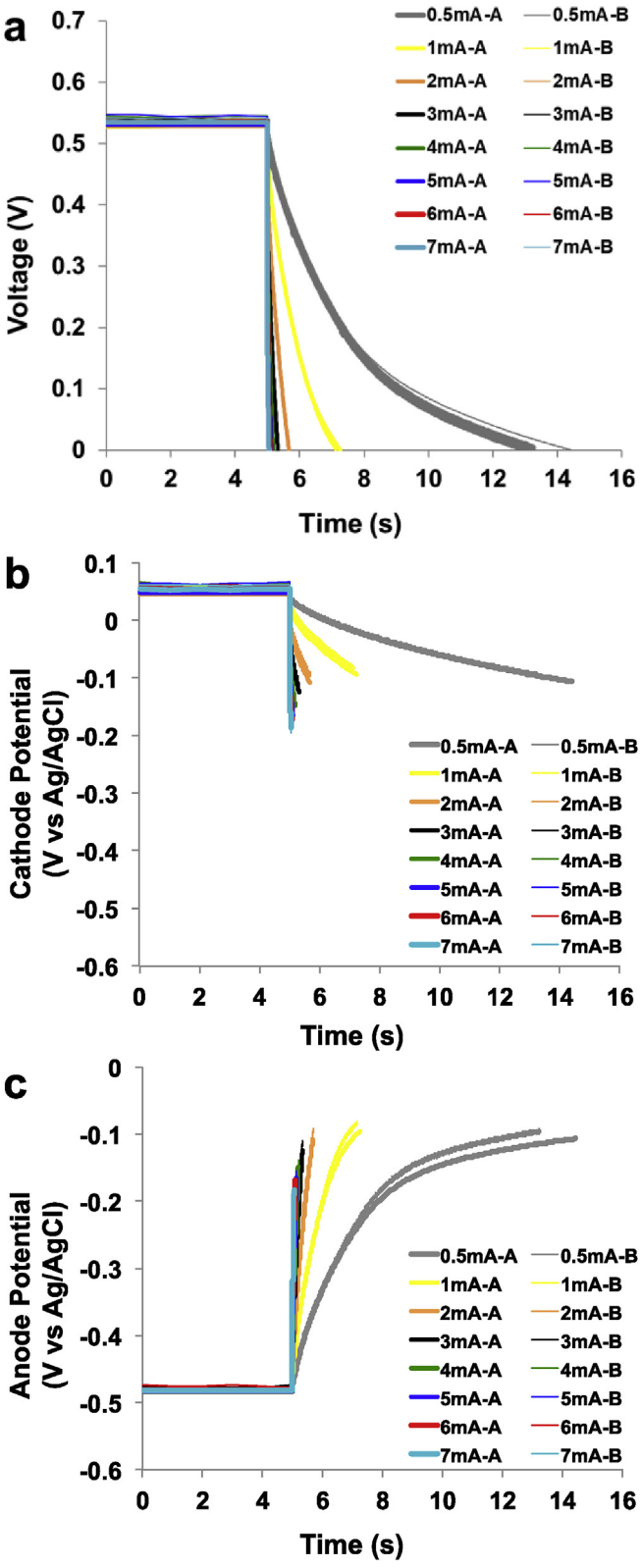

Fig. 3. Complete discharges for SC-MFC-2C at different i_{pulse}. Overall (a), cathode (b), anode (c) profile during the discharge. A and B are the two separate SC-MFCs.

3.3. Effect of addition of supercapacitive features into the anode

The cathode ohmic resistance (R_C) was diminished by adding the second cathode as discussed in the previous section. The next strategy adopted to enhance the performance was to add a supercapacitive layer made by a mixture of AC and PTFE and embedded within the carbon veil anode. Complete GLV discharges for SC-MFC-2CCA were presented in Fig. 4.

The OCV remained comparable compared to SC-MFC-2C measuring 527 ± 7 mV. In this case, the overall ESR increased measuring 49.03 ± 1.08 Ω with R_A being 26.33 ± 2.20 Ω and R_C being 22.71 ± 2.39 Ω. R_C remained almost stable compared to the previous set of SC-MFCs while R_A increased by roughly 10 Ω. This might be due to a worse connection or to the presence of PTFE that decreased the electrode conductivity. Despite higher ESR, t_{pulse} for complete discharge increased for any i_{pulse} investigated (Table S3). Particularly, at i_{pulse} of 2 mA, t_{pulse} was 24.54 ± 1.63 s, which was much higher compared to SC-MFC-C and SC-MFC-2C. At the higher i_{pulse} investigated (7 mA), t_{pulse} was 0.12 ± 0.03 s (Table S3). Overall apparent capacitance values and the one of each single electrode are reported in Table S3. For low i_{pulse} (2 mA), only the initial linear part was considered in the apparent capacitance calculation. Also in this case, the apparent capacitance increased with the decreasing i_{pulse} and the values recorded varied between 36.37 ± 0.31 mF (i_{pulse} 2 mA) and 4.86 ± 0.82 mF (i_{pulse} 7 mA). With the addition of capacitive features on the anode, its apparent capacitance improved significantly. In this case, the apparent capacitance was higher compared to the one of the cathode (Table S3) being beneficial for the overall capacitance.

3.4. Effect of series and parallel connection during the galvanostatic discharges

In the previous paragraph, the overall electrochemical performance during galvanostatic discharges were improved by firstly doubling the cathode area and then by adding capacitive features within the anode electrode. The SC-MFC-2CCAs (double cathode and capacitive anodes) were then connected firstly in parallel and then in series and complete GLV discharges were conducted. Unfortunately, the trend of each single electrode using a reference electrode could not be monitored due to the fact that the two SC-MFCs were hydraulically disconnected. Complete discharges with SC-MFC-2CCAs connected in series are shown in Fig. 5.a. Instead, complete discharges with SC-MFC-2CCAs connected in parallel are shown in Fig. 5.b.

Parameters of interests such as i_{pulse}, ESR, discharge time and apparent capacitance are summarized in Table 2. Concerning the series connection, OCV almost doubled measuring 1050 ± 9 mV and ESR was 75.0 ± 0.9 Ω. Discharge time varied between 0.03 s (i_{pulse} 10 mA) and 21.77 s (i_{pulse} 2 mA). Apparent capacitance also varied between 0.72 mF (i_{pulse} 10 mA) and 16.15 mF (i_{pulse} 2 mA). The connection series enhanced the operating voltage but did not contribute on increasing the time of discharge. Parallel connection led to an OCV of 525 ± 5 mV and an ESR of 22.7 ± 0.4 Ω. Discharge time increased substantially at lower current pulse. The apparent capacitance improved importantly achieving the higher value of 62.99 mF (i_{pulse} 4 mA).

The Ragone plots related to SC-MFC-Cs, SC-MFC-2Cs and SC-MFC-2CCAs are reported in Figure S1.a. The Ragone plots related to SC-MFC-2CCAs connected in series and parallel are reported in Figure S1.b. The Ragone plots are used to compare the energy and power output for each type of SC-MFC. For each system, the highest energy was delivered at the lowest current. The energy delivered at i_{pulse} equal to 2 mA by SC-MFC-2CCAs was 3.3 ± 0.1 mJ.

It can be seen that SC-MFC-2C is performing better than SC-

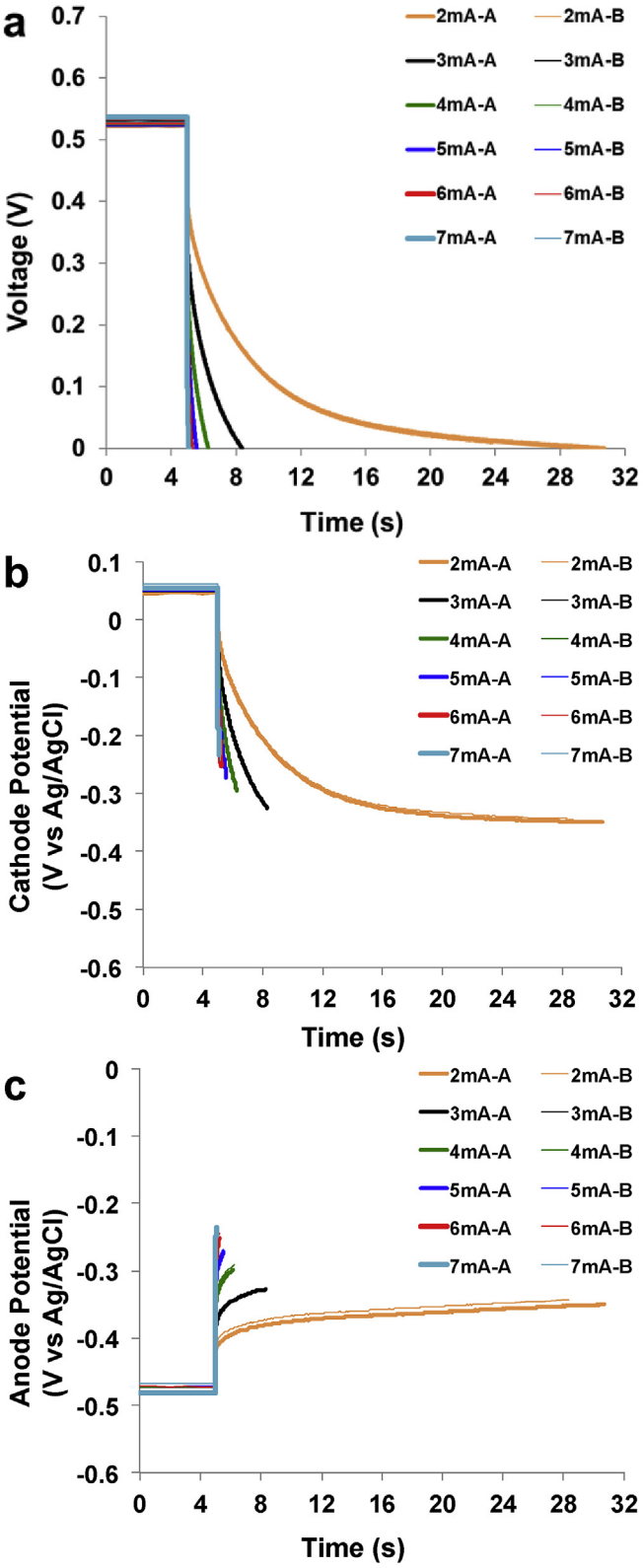

Fig. 4. Complete discharges for SC-MFC-2CCA at different i_{pulse}. Overall (a), cathode (b), anode (c) profile during the discharge. A and B are the two separate SC-MFCs.

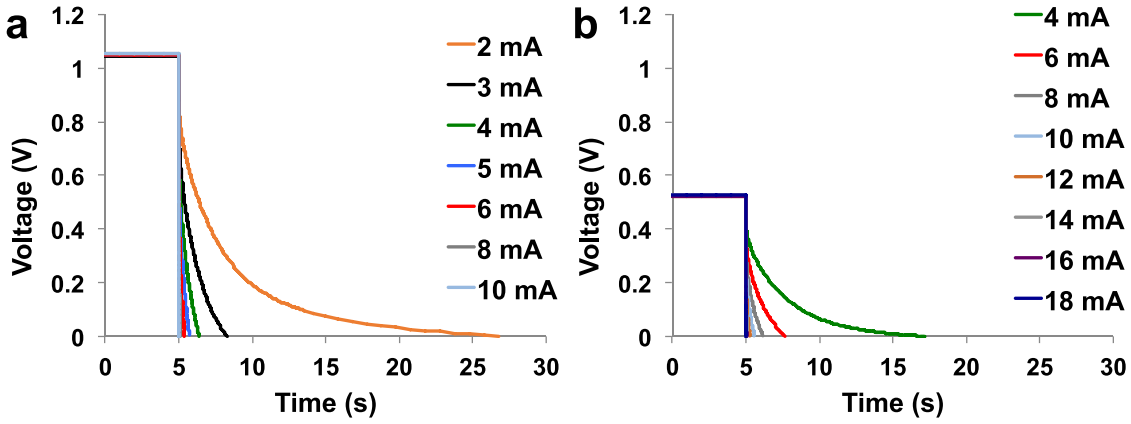

Fig. 5. Complete discharges at different i_{pulse} for SC-MFC-2CCA connected in series (a) and in parallel (b).

Table 2
ESR, discharge time and apparent capacitance for SC-MFC-2CCAs connected in series or parallel.

Series		discharge	apparent	Parallel		discharge	apparent
i_{pulse}	ESR	time	C_{tot}	i_{pulse}	ESR	time	C_{tot}
mA	Ω	s	mF	mA	Ω	s	mF
2	73.3	21.77	16.15	4	23	12.20	62.99
3	75.6	3.31	12.17	6	23	2.71	42.60
4	75.9	1.39	7.48	8	22.8	1.17	27.51
5	74.9	0.75	5.53	10	22.7	0.58	19.46
6	75.1	0.40	3.99	12	22.9	0.27	13.02
7	74.3	0.23	3.07	14	22.8	0.13	9.15
8	74.7	0.12	2.09	16	22.7	0.06	5.84
10	74.4	0.03	0.72	18	22.6	0.02	3.57
	75.0 ± 0.9				22.7 ± 0.4		

MFC-C for t_{pulse} lower than 1 s but for higher time they performed similarly. This might be due to the fact that SC-MFC-2C had lower ESR but also lower OCV. Interestingly, the best performance were achieved by SC-MFC-2CCA for t_{pulses} higher than 0.5 s. At low t_{pulse}, the low OCV and its ESR affected negatively the performance of SC-MFC-2CCA. At higher t_{pulse}, the faradaic contribution allowed it to achieve superior performance. The connection in series and in parallel brought to similar curves on the Ragone plots (Figure S1.b) with much superior performance compared to the single SC-MFC-2CCA indicating that the stacking in series or in parallel is a beneficial way for improving the output.

3.5. Power curves

Power curves for SC-MFC-C (Fig. 6a), SC-MFC-2C (Fig. 6b) and SC-MFC-2CCA (Fig. 6c) at different t_{pulses} were presented. Higher power was obtained by SC-MFC-2C at shorter t_{pulse} with values recorded of 1.59 ± 0.01 mW (1.06 ± 0.01 mW mL^{-1}) and 1.17 ± 0.02 mW (0.78 ± 0.01 mW mL^{-1}) at discharge time of 0.01 s and 0.05 s respectively. At t_{pulse} higher than 0.25 s, despite higher ESR and similar OCV, the higher power was achieved by SC-MFC-2CCA because of its higher apparent capacitance. Particularly, the peak of power recorded for SC-MFC-2CCA at t_{pulse} of 0.25 s, 0.5 s, 1 s and 2 s was 0.86 ± 0.02 mW (0.58 ± 0.01 mW mL^{-1}), 0.78 ± 0.01 mW (0.52 ± 0.01 mW mL^{-1}), 0.65 ± 0.00 mW (0.44 ± 0.00 mW mL^{-1}) and 0.57 ± 0.01 mW (0.38 ± 0.01 mW mL^{-1}), respectively.

The power curves obtained at different t_{pulse} for SC-MFC-2CCA connected in series and in parallel are instead shown in Fig. 7a and 7.b respectively. The peaks of power curves are reported in Table S4. Generally, the peak of power is greater for the series connection despite it occurring at lower current. As expected, the current delivered by the parallel connection of the two SC-MFC-2CCAs is greater compared to the series connection of the latters.

3.6. Durability tests

Longevity tests of discharge self-recharge were conducted in order to study the durability of the system. Discharges were done delivering an i_{pulse} of 2 mA for a t_{pulse} of 1 s. Discharges were followed by a period of rest of 120 s in which the cell was disconnected and no current was flowing within the circuit. In this case, the electrodes were self-recharged due to the anaerobic/aerobic environments occurring in the proximity of the two electrodes, anode and cathode respectively. 4000 cycles of discharges/self-recharges were conducted for a lapse of time equivalent to ≈135 h (≈5.6 days). The overall voltage trend during the durability test is reported in Figure S2.a while the separate anode and cathode potential trends are reported in Figure S2.b and S2.c, respectively. In order to study the durability of the system, cycle number 200, 1000, 2000, 3000 and 4000 were separate from the overall test and reported in Fig. 8. Particularly, cell voltage, cathode potential and anode potential at these specific cycles were reported in Fig. 8.a, Fig. 8.b and Fig. 8.c respectively. Data measured for OCV, OCP_a, OCP_c, ESR, R_A, R_C, C_{cell}, C_A and C_C recorded for cycle 200, 1000, 2000, 3000 and 4000 were also reported in Table S5. OCV varied slightly between 501 mV (cycle 2000) and 516 mV (cycle 4000) (Fig. 8a). The cathode OCP tended to decrease as well except for the last cycle where it was slightly higher than the value recorded after 3000 cycles (Fig. 8b). The anodic OCP tended to decrease over the 4000

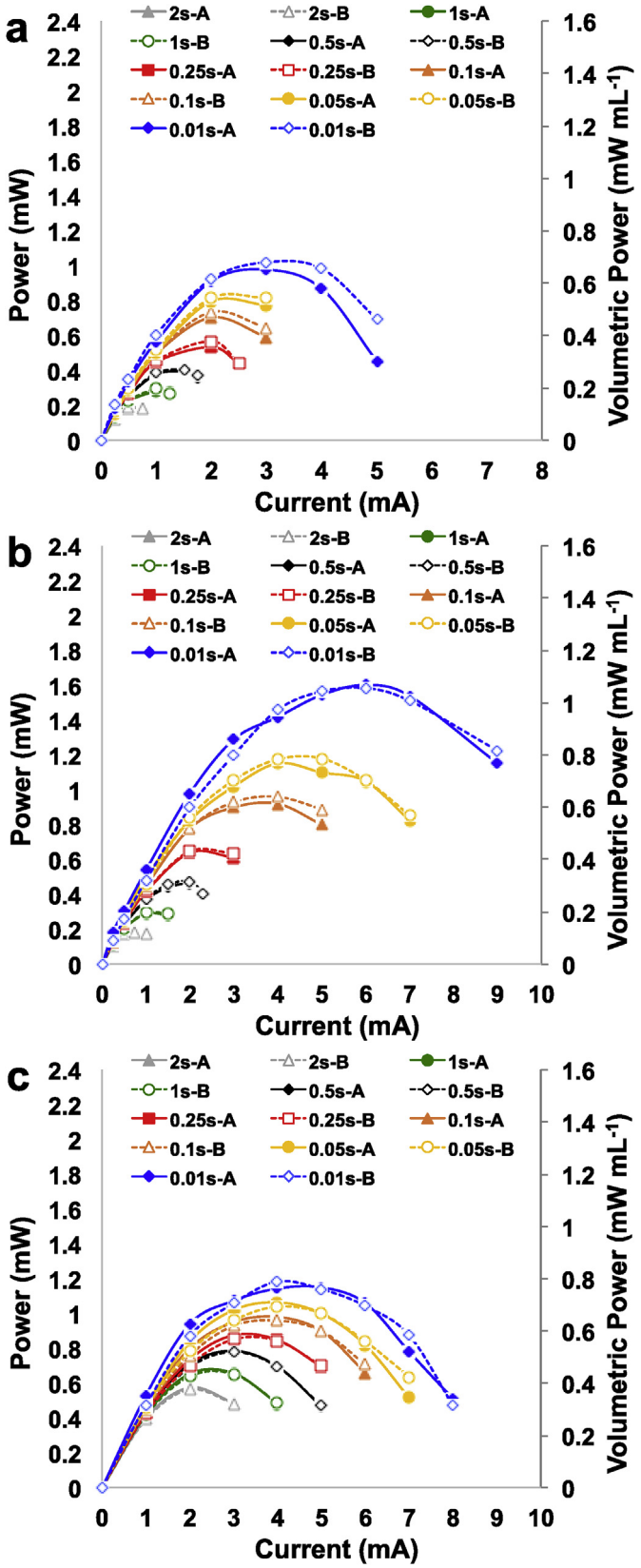

Fig. 6. Power curves for SC-MFC-C (a), SC-MFC-2C (b) and SC-MFC-2C-CA (c) considering t_{pulse} of 2 s, 1 s, 0.5 s, 0.25 s, 0.1 s, 0.05 s and 0.01 s. A and B are the two separate SC-MFCs.

cycles varying from an initial value of −459 mV (vs Ag/AgCl) to a value of −480 mV (vs Ag/AgCl) (Fig. 8c). From these measurements, it seems that both the anodic and cathodic potentials were decreasing over time. This can be explained by the biofilm formation and biofouling occurring on the cathode electrodes in a short amount of time as previously reported [94–96]. This biofilm/biofouling layer might have lowered the oxygen penetration within the anodic chamber reducing the negative effect on the anode, which became more negative over time due to more established anaerobic environments. Better biofilm adaptation and better anode colonisation might also be important points to consider.

ESR values increased from 51.4 Ω (cycle 200) to 55.7 Ω (cycle 3000) and the slightly decrease in the last cycle (52.9 Ω) (Table S5). The anodic resistance increased over the cycles as well as the cathodic one except the last cycle in which a decrease of 3.4 Ω was measured (Table S5). In parallel, also the apparent capacitance measured for the entire cell decreased over the first 3000 cycles and then slightly increased at cycle 4000 (Table S5). The anodic apparent capacitance decreased over the cycles while the cathodic apparent capacitance followed the trend of the overall apparent capacitance. Generally, it can be notice a slight decrease in ESR and apparent capacitance underlining a slow deterioration of the operating conditions. Interestingly, it can be noticed a decrease in performance around 3500 cycles (Figure S2.a) and this was probably due to the formation/creation of an air-bubble inside the anodic chamber and this might have decreased the anode area exposed to the electrolyte or temporarily negatively affect the anaerobiosis condition within the anode electrode. An increase in the anode potential can be in fact noticed around cycle 3500. Once the problem was identified, the operator removed the bubble and the condition re-established similar to previous conditions. Actually, the removal of the air-bubble enhanced the cathode performance which ESR and apparent capacitance increased during cycle 4000. This was beneficial also to the overall SC-MFC, which recovered part of its losses.

3.7. Overview of the current study

In this study, a small air-breathing cathode membraneless MFC with a displacement volume of 1.5 mL was operated in supercapacitive mode. Initially, it was tested using the same materials usually adopted for MFCs operating in standard mode under a constant load. In fact, carbon veil anode and activated carbon-based cathode were adopted. ESR was relatively high mainly due to the cathode electrode and the capacitance of the SC-MFC was very low especially due to the poor capacitance of the carbon veil. In order to boost the performance up, a second cathode was accommodated and a capacitive layer was added to the anode electrode. This double variation led to a decrease in the cathode resistance and therefore overall ESR and to an enhancement of the anode apparent capacitance and therefore the overall SC-MFC apparent capacitance. Unfortunately, both variations had their own negative effect. The addition of the second cathode decreased the SC-MFC OCV probably influencing negatively the anaerobic environment of the anode. The addition of the capacitive features on the anode increased the anodic and overall resistance. It was shown that at shorter discharge time, SC-MFC with double cathode was the best performing with the highest peak of power recorded in this study of 1.59 ± 0.01 mW (1.06 ± 0.01 mW mL^{-1}). At longer discharge time, SC-MFC with double cathode and modified anode had the higher power produced (0.57 ± 0.01 mW corresponding to 0.38 ± 0.01 mW mL^{-1}) and higher apparent capacitance. Despite being pulsed power and not continuous, the output is more than one order of magnitude higher compared to similar MFCs operating in continuous mode. The decrease in the reactor size compared to

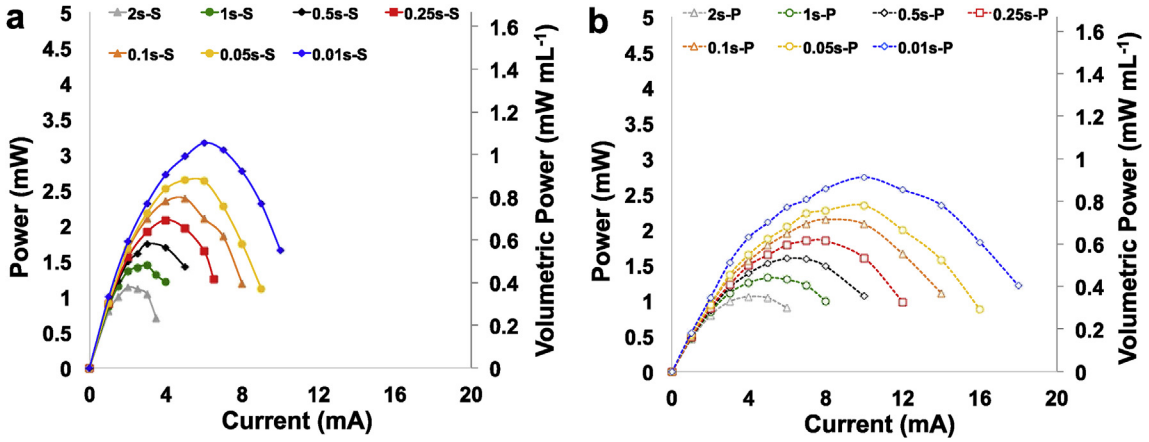

Fig. 7. Power curves for two SC-MFC-2C–CAs connected in series (a) and in parallel (b) considering t_{pulse} of 2 s, 1 s, 0.5 s, 0.25 s, 0.1 s, 0.05 s and 0.01 s.

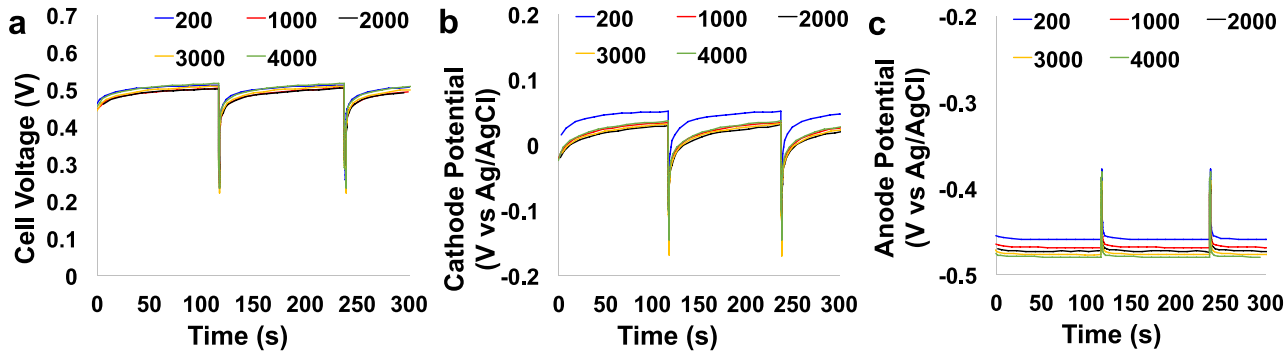

Fig. 8. Durability test of a single SC-MFC-2CCA for 4000 cycles of discharge at i_{pulse} of 2 mA and self-recharge. Overall voltage (a), cathode potential (b) and anode potential (c) recorded for cycle 200, 1000, 2000, 3000 and 4000.

previously presented literature showed an increase in power produced [97,98]. As the reactor become smaller, electrode area to volume ratio is optimised, less planktonic and competitive bacteria are present into the systems and distances between electrodes decreases affecting positively the ohmic resistances that are reduced.

At lower discharge current, the faradaic contribution became predominant in agreement with previously presented results [80,90]. Another strategy for enhancing the electrochemical performance is to connect different SC-MFC in series or in parallel. Series connection allows boosting the operating voltage. Parallel connection instead is necessary to improve current generated. The connection in Series or Parallel of two SC-MFCs led to similar power output despite the series connection being slightly more performing. Similar powers generated were obtained even if the connection in parallel allowed reaching almost double current compared to the series connection. Durability tests showed that the system was robust over 4000 cycles despite a light decrease in the parameters of interest.

4. Conclusions

Membraneless SC-MFC with air-breathing cathode was tested in supercapacitive mode. Hydrolysed human urine was used as feeding as well as electrolyte. Control SC-MFC having carbon veil anode and AC/PTFE cathode was subject to galvanostatic discharges. The performance was improved by doubling the cathode leading to a diminishment of the ESR and improvement in the apparent capacitance. The performance was improved even more by embedding AC-based capacitive features in the anode electrode. Maximum power output obtained was 1.59 ± 0.01 mW (1.06 ± 0.01 mW mL^{-1}) at t_{pulse} of 0.01 s and 0.57 ± 0.01 mW (0.38 ± 0.01 mW mL^{-1}) at t_{pulse} of 2 s. The apparent capacitance increased significantly with the decrease of discharge current applied indicating the presence of the faradaic component during the discharge. The higher apparent capacitance recorded in this work considering the initial linear voltage decrease was 36.37 ± 0.31 mF. Connection in series and parallel between different SC-MFC help improve the performance with the series connection enhancing the overall voltage and the parallel connection instead increasing the current delivered. SC-MFC was also discharged and self-recharged for 4000 cycles showing robustness. Compared with previous work, reducing the size of the reactor clearly boosts the volumetric power output.

Credit author statement

Carlo Santoro: Conceptualization, Methodology, Data curation, Analysis and Interpretation, Investigation, Writing-Original draft preparation, Xavier Alexis Walter: Methodology, Investigation, Data curation, Analysis and Interpretation, Writing- Reviewing. Francesca Soavi: Data Analysis and Interpretation, Writing-Reviewing and Editing, John Greenman: Supervision, Writing-Reviewing and Editing, Ioannis Ieropoulos: Supervision, Funding acquisition, Writing-Reviewing and Editing.

Declaration of competing interest

The authors declare that they have no known competing financial interests that could have appeared to influence the work reported in this paper.

Acknowledgements

CS would like to acknowledge the financial support from the Bristol BioEnergy Centre QR (UWE internal fund) for funding certain aspects of this work. IAI and XAW would like to acknowledge the Bill & Melinda Gates Foundation (grant no. OPP1149065) for the support and for funding parts of this work. F.S. acknowledges the Italian Minister of Foreign Affairs and the Ministry of the Environment, Land and Sea of the Republic of Italy under the Italy South Africa Research Project (ISARP) 2018–2020 - Progetto di Grande Rilevanza.

Appendix A. Supplementary data

Supplementary data to this article can be found online at https://doi.org/10.1016/j.electacta.2020.136530.

References

[1] S. Bajracharya, S. Srikanth, G. Mohanakrishna, R. Zacharia, D.P. Strik, D. Pant, Biotransformation of carbon dioxide in bioelectrochemical systems: state of the art and future prospects, J. Power Sources 356 (2017) 256–273.
[2] M. Rahimnejad, A. Adhami, S. Darvari, A. Zirepour, S.E. Oh, Microbial fuel cell as new technology for bioelectricity generation: a review, Alexandria Eng. J. 54 (2015) 745–756.
[3] A. Rinaldi, B. Mecheri, V. Garavaglia, S. Licoccia, P. Di Nardo, E. Traversa, Engineering materials and biology to boost performance of microbial fuel cells: a critical review, Energy Environ. Sci. 1 (2008) 417–429.
[4] C. Santoro, C. Arbizzani, B. Erable, I. Ieropoulos, Microbial fuel cells: from fundamentals to applications. A review, J. Power Sources 356 (2017) 225–244.
[5] S. Bajracharya, M. Sharma, G. Mohanakrishna, X.D. Benneton, D.P. Strik, P.M. Sarma, D. Pant, An overview on emerging bioelectrochemical systems (BESs): technology for sustainable electricity, waste remediation, resource recovery, chemical production and beyond, Renew. Energy 98 (2016) 153–170.
[6] P. Pandey, V.N. Shinde, R.L. Deopurkar, S.P. Kale, S.A. Patil, D. Pant, Recent advances in the use of different substrates in microbial fuel cells toward wastewater treatment and simultaneous energy recovery, Appl. Energy 168 (2016) 706–723.
[7] D. Pant, G. Van Bogaert, L. Diels, K. Vanbroekhoven, A review of the substrates used in microbial fuel cells (MFCs) for sustainable energy production, Bioresour. Technol. 101 (2010) 1533–1543.
[8] Y.H.M.S.M. Annuar, A.M. Gumel, Mini-review: anode modification for improved performance of microbial fuel cell, Renew. Sustain. Energy Rev. 73 (2017) 236–248.
[9] J. Wei, P. Liang, X. Huang, Recent progress in electrodes for microbial fuel cells, Bioresour. Technol. 102 (2011) 9335–9344.
[10] A. ElMekawy, H.M. Hegab, D. Losic, C.P. Saint, D. Pant, Applications of graphene in microbial fuel cells: the gap between promise and reality, Renew. Sustain. Energy Rev. 72 (2017) 1389–1403.
[11] S. Chen, S.A. Patil, R.K. Brown, U. Schröder, Strategies for optimizing the power output of microbial fuel cells: transitioning from fundamental studies to practical implementation, Appl. Energy 233 (2019) 15–28.
[12] E. Antolini, Composite materials for polymer electrolyte membrane microbial fuel cells, Biosens. Bioelectron. 69 (2015) 54–70.
[13] Z. Du, H. Li, T. Gu, A state of the art review on microbial fuel cells: a promising technology for wastewater treatment and bioenergy, Biotechnol. Adv. 25 (2007) 464–482.
[14] K. Guo, A. Prévoteau, S.A. Patil, K. Rabaey, Engineering electrodes for microbial electrocatalysis, Curr. Opin. Biotechnol. 33 (2015) 149–156.
[15] K. Guo, S. Freguia, P.G. Dennis, X. Chen, B.C. Donose, J. Keller, J.J. Gooding, K. Rabaey, Effects of surface charge and hydrophobicity on anodic biofilm formation, community composition, and current generation in bioelectrochemical systems, Environ. Sci. Technol. 47 (2013) 7563–7570.
[16] E. Blanchet, B. Erable, M.L. De Solan, A. Bergel, Two-dimensional carbon cloth and three-dimensional carbon felt perform similarly to form bioanode fed with food waste, Electrochem. Commun. 66 (2016) 38–41.
[17] S. Li, C. Cheng, A. Thomas, Carbon-based microbial-fuel-cell electrodes: from conductive supports to active catalysts, Adv. Mater. 29 (2017), 1602547.
[18] J.M. Sonawane, A. Yadav, P.C. Ghosh, S.B. Adeloju, Recent advances in the development and utilization of modern anode materials for high performance microbial fuel cells, Biosens. Bioelectron. 90 (2017) 558–576.
[19] B. Erable, N. Byrne, L. Etcheverry, W. Achouak, A. Bergel, Single medium microbial fuel cell: stainless steel and graphite electrode materials select bacterial communities resulting in opposite electrocatalytic activities, Int. J. Hydrogen Energy 42 (2017) 26059–26067.
[20] J. You, C. Santoro, J. Greenman, C. Melhuish, P. Cristiani, B. Li, I. Ieropoulos, Micro-porous layer (MPL)-based anode for microbial fuel cells, Int. J. Hydrogen Energy 39 (2014) 21811–21818.
[21] M. Oliot, L. Etcheverry, A. Mosdale, R. Basseguy, M.-L. Delia, A. Bergel, Separator electrode assembly (SEA) with 3-dimensional bioanode and removable air-cathode boosts microbial fuel cell performance, J. Power Sources 356 (2017) 389.
[22] M. Grattieri, N.D. Shivel, I. Sifat, M. Bestetti, S.D. Minteer, Sustainable hypersaline microbial fuel cells: inexpensive recyclable polymer supports for carbon nanotube conductive paint anodes, ChemSusChem 10 (2017) 2053–2058.
[23] E. Guerrini, P. Cristiani, M. Grattieri, C. Santoro, B. Li, S. Trasatti, Electrochemical behavior of stainless steel anodes in membraneless microbial fuel cells, J. Electrochem. Soc. 161 (2014) H62–H67.
[24] A. Baudler, I. Schmidt, M. Langner, A. Greiner, U. Schröder, Does it have to be carbon? Metal anodes in microbial fuel cells and related bioelectrochemical systems, Energy Environ. Sci. 8 (2015) 2048–2055.
[25] U. Michaelidou, A. ter Heijne, G.J.W. Euverink, H.V.M. Hamelers, A.J.M. Stams, J.S. Geelhoed, Microbial communities and electrochemical performance of titanium-based anodic electrodes in a microbial fuel cell, Appl. Environ. Microbiol. 77 (2011) 1069–1075.
[26] D. Pocaznoi, A. Calmet, L. Etcheverry, B. Erable, A. Bergel, Stainless steel is a promising electrode material for anodes of microbial fuel cells, Energy Environ. Sci. 5 (2012) 9645–9652.
[27] S.F. Ketep, A. Bergel, A. Calmet, B. Erable, Stainless steel foam increases the current produced by microbial bioanodes in bioelectrochemical systems, Energy Environ. Sci. 7 (2014) 1633–1637.
[28] T. Yamashita, H. Yokoyama, Molybdenum anode: a novel electrode for enhanced power generation in microbial fuel cells, identified via extensive screening of metal electrodes, Biotechnol. Biofuels 11 (2018) 39.
[29] Z. Wang, C. Cao, Y. Zheng, S. Chen, F. Zhao, Abiotic oxygen reduction reaction catalysts used in microbial fuel cells, ChemElectroChem 1 (2014) 1813.
[30] Z. Wang, G.D. Mahadevan, Y. Wu, F. Zhao, Progress of air-breathing cathode in microbial fuel cells, J. Power Sources 356 (2017) 245.
[31] H. Yuan, Y. Hou, I.M. Abu-Reesh, J. Chen, Z. He, Oxygen reduction reaction catalysts used in microbial fuel cells for energy-efficient wastewater treatment: a review, Mater. Horiz. 3 (2016) 382–401.
[32] S. Rojas-Carbonell, K. Artyushkova, A. Serov, C. Santoro, I. Matanovic, P. Atanassov, Effect of pH on the activity of platinum group metal-free catalysts in oxygen reduction reaction, ACS Catal. 8 (2018) 3041–3053.
[33] D. Malko, A. Kucernak, T. Lopes, In situ electrochemical quantification of active sites in Fe–N/C non-precious metal catalysts, Nat. Commun. 7 (2016) 13285.
[34] K. Kinoshita, Electrochemical Oxygen Technology, John Wiley Sons, New York, NY, 1992.
[35] W. Yang, K.Y. Kim, P.E. Saikaly, B.E. Logan, The impact of new cathode materials relative to baseline performance of microbial fuel cells all with the same architecture and solution chemistry, Energy Environ. Sci. 10 (2017) 1025–1033.
[36] W. Yang, J. Li, L. Lan, Q. Fu, L. Zhang, X. Zhu, Q. Liao, Poison tolerance of non-precious catalyst towards oxygen reduction reaction, Int. J. Hydrogen Energy 43 (2018) 8474–8479.
[37] M. Kodali, R. Gokhale, C. Santoro, A. Serov, K. Artyushkova, P. Atanassov, High performance platinum group metal-free cathode catalysts for microbial fuel cell (MFC), J. Electrochem. Soc. 164 (2017) H3041–H3046.
[38] N. Duteanu, B. Erable, S.M.S. Kumar, M.M. Ghangrekar, K. Scott, Effect of chemically modified Vulcan XC-72R on the performance of air-breathing cathode in a single-chamber microbial fuel cell, Bioresour. Technol. 101 (2010) 5250–5255.
[39] H. Dong, H. Yu, H. Yu, N. Gao, X. Wang, Enhanced performance of activated carbon–polytetrafluoroethylene air-cathode by avoidance of sintering on catalyst layer in microbial fuel cells, J. Power Sources 232 (2013) 132–138.
[40] X.A. Walter, J. Greenman, I. Ieropoulos, Binder materials for the cathodes applied to self-stratifying membraneless microbial fuel cell, Bioelectrochemistry 123 (2018) 119–124.
[41] F. Zhang, D. Pant, B.E. Logan, Long-term performance of activated carbon air cathodes with different diffusion layer porosities in microbial fuel cells, Biosens. Bioelectron. 30 (2011) 49–55.
[42] S. Sevda, X. Dominguez-Benetton, K. Vanbroekhoven, H. De Wever, T.R. Sreekrishnan, D. Pant, High strength wastewater treatment accompanied by power generation using air cathode microbial fuel cell, Appl. Energy 105 (2013) 194–206.
[43] I. Merino-Jimenez, C. Santoro, S. Rojas-Carbonell, J. Greenman, I. Ieropoulos, P. Atanassov, Carbon-based air-breathing cathodes for microbial fuel cells, Catalysts 6 (2016) 127.
[44] R. Rossi, P.J. Evans, B.E. Logan, Impact of flow recirculation and anode dimensions on performance of a large scale microbial fuel cell, J. Power Sources 412 (2019) 294–300.
[45] C. Santoro, M.R. Talarposhti, M. Kodali, R. Gokhale, A. Serov, I. Merino-Jimenez, I. Ieropoulos, P. Atanassov, Microbial desalination cells with efficient platinum-group-metal-free cathode catalysts, ChemElectroChem 4 (2017) 3322–3330.

[46] C. Santoro, M. Kodali, S. Herrera, A. Serov, I. Ieropoulos, P. Atanassov, Power generation in microbial fuel cells using platinum group metal-free cathode catalyst: effect of the catalyst loading on performance and costs, J. Power Sources 378 (2018) 169–175.

[47] M. Kodali, C. Santoro, S. Herrera, A. Serov, P. Atanassov, Bimetallic platinum group metal-free catalysts for high power generating microbial fuel cells, J. Power Sources 366 (2017) 18–26.

[48] C. Santoro, S. Rojas-Carbonell, R. Awais, R. Gokhale, M. Kodali, A. Serov, K. Artyushkova, P. Atanassov, Influence of platinum group metal-free catalyst synthesis on microbial fuel cell performance, J. Power Sources 375 (2018) 11–20.

[49] M. Kodali, S. Herrera, S. Kabir, A. Serov, C. Santoro, I. Ieropoulos, P. Atanassov, Enhancement of microbial fuel cell performance by introducing a nano-composite cathode catalyst, Electrochim. Acta 265 (2018) 56–64.

[50] B. Erable, M. Oliot, R. Lacroix, A. Bergel, A. Serov, M. Kodali, C. Santoro, P. Atanassov, Iron-Nicarbazin derived platinum group metal-free electro-catalyst in scalable-size air-breathing cathodes for microbial fuel cells, Electrochim. Acta 277 (2018) 127–135.

[51] R. Rossi, W. Yang, L. Setti, B.E. Logan, Assessment of a metal–organic framework catalyst in air cathode microbial fuel cells over time with different buffers and solutions, Bioresour. Technol. 233 (2017) 399–405.

[52] W. Yang, X. Wang, R. Rossi, B.E. Logan, Low-cost Fe–N–C catalyst derived from Fe (III)-chitosan hydrogel to enhance power production in microbial fuel cells, Chem. Eng. J. 380 (2020), 122522.

[53] C. Santoro, R. Gokhale, B. Mecheri, A. D'Epifanio, S. Licoccia, A. Serov, K. Artyushkova, P. Atanassov, Design of iron(II) pthalocyanine (FePc) derived oxygen reduction electrocatalysts for high power density microbial fuel cells, ChemSusChem 10 (2017) 3243–3251.

[54] M.-T. Nguyen, B. Mecheri, A. Iannaci, A. D'Epifanio, S. Licoccia, Iron/Polyindole-based electrocatalysts to enhance oxygen reduction in microbial fuel cells, Electrochim. Acta 190 (2016) 388–395.

[55] M.A. Costa de Oliveira, B. Mecheri, A. D'Epifanio, E. Placidi, F. Arciprete, F. Valentini, A. Perandini, V. Valentini, S. Licoccia, Graphene oxide nanoplatforms to enhance catalytic performance of iron phthalocyanine for oxygen reduction re- action in bioelectrochemical systems, J. Power Sources 356 (2017) 381–388.

[56] F. Shahbazi Farahani, B. Mecheri, M. Reza Majidi, M.A. Costa de Oliveira, A. D'Epifanio, F. Zurlo, E. Placidi, F. Arciprete, S. Licoccia, MnOx-based electrocatalysts for enhanced oxygen reduction in microbial fuel cell air cathodes, J. Power Sources 390 (2018) 45–53.

[57] M. Kodali, C. Santoro, A. Serov, S. Kabir, K. Artyushkova, I. Matanovic, P. Atanassov, Air breathing cathodes for microbial fuel cell using Mn-, Fe-, Co- and Ni-containing platinum group metal-free catalysts, Electrochim. Acta 231 (2017) 115–124.

[58] F.L. Lobo, X. Wang, Z.J. Ren, Energy harvesting influences electrochemical performance of microbial fuel cells, J. Power Sources 356 (2017) 356–364.

[59] H.C. Boghani, R.M. Dinsdale, A.J. Guwy, G.C. Premier, Sampled-time control of a microbial fuel cell stack, J. Power Sources 356 (2017) 338–347.

[60] H. Wang, J.D. Park, Z.J. Ren, Practical energy harvesting for microbial fuel cells: a review, Environ. Sci. Technol. 49 (2015) 3267–3277.

[61] S. Wilkinson, "Gastrobots"—benefits and challenges of microbial fuel cells in FoodPowered robot applications, Aut. Robots 9 (2000) 99–111.

[62] I. Ieropoulos, C. Melhuish, J. Greenman, Artificial metabolism: towards true energetic autonomy in artificial life, Adv. Artificial Life, Proc. 2801 (2003) 792–799.

[63] I. Ieropoulos, C. Melhuish, J. Greenman, I. Horsfield EcoBot, An artificial agent with a natural metabolism, Int. J. Adv. Rob. Syst. 2 (2005) 295–300.

[64] I. Ieropoulos, J. Greenman, C. Melhuish, I. Horsfield EcoBot, A robot with guts, 12th Int. Conf. Synth. Simul. Living Syst. (2010) 733–740.

[65] F. Soavi, L.G. Bettini, P. Piseri, P. Milani, C. Santoro, P. Atanassov, C. Arbizzani, Miniaturized supercapacitors: key materials and structures towards autonomous and sustainable devices and systems, J. Power Sources 326 (2016) 717–725.

[66] J. Houghton, C. Santoro, F. Soavi, A. Serov, I. Ieropoulos, C. Arbizzani, P. Atanassov, Supercapacitive microbial fuel cell: characterization and analysis for improved charge storage/delivery performance, Bioresour. Technol. 218 (2016) 552–560.

[67] C. Santoro, F. Soavi, C. Arbizzani, A. Serov, S. Kabir, K. Carpenter, O. Bretschger, P. Atanassov, Co-generation of hydrogen and power/current pulses from supercapacitive MFCs using novel HER iron-based catalysts Electrochim, Acta 220 (2016) 672–682.

[68] C. Santoro, J. Winfield, P. Theodosiou, I. Ieropoulos, Supercapacitive paper based microbial fuel cell: high current/power production within a low cost design, Bioresour. Technol. Rep. 7 (2019), 100297.

[69] C. Santoro, F. Soavi, A. Serov, C. Arbizzani, P. Atanassov, Self-powered supercapacitive microbial fuel cell: the ultimate way of boosting and harvesting power, Biosens. Bioelectron. 78 (2016) 229–235.

[70] C. Santoro, M. Kodali, S. Kabir, F. Soavi, A. Serov, P. Atanassov, Three-dimensional graphene nanosheets as cathode catalysts in standard and supercapacitive microbial fuel cell, J. Power Sources 356 (2017) 371–380.

[71] F. Soavi, C. Santoro, Supercapacitive operational mode in microbial fuel cell, Curr. Opin. Electrochem. 22 (2020) 1–8.

[72] A. Deeke, T.H.J.A. Sleutels, A. Ter Heijne, H.V.M. Hamelers, C.J.N. Buisman, Influence of the thickness of the capacitive layer on the performance of bioanodes in microbial fuel cells, J. Power Sources 243 (2013) 611–616.

[73] C. Borsje, D. Liu, T.H.J.A. Sleutels, C.J.N. Buisman, A. Ter Heijne, Performance of single carbon granules as perspective for larger scale capacitive bioanodes, J. Power Sources 325 (2016) 690–696.

[74] L. Caizán-Juanarena, I. Servin-Balderas, X. Chen, C.J.N. Buisman, A. ter Heijne, Electrochemical and microbiological characterization of single carbon granules in a multi-anode microbial fuel cell, J. Power Sources 435 (2019), 126514.

[75] C. Borsje, T. Sleutels, M. Saakes, C.J.N. Buisman, A. ter Heijne, The granular capacitive moving bed reactor for the scale up of bioanodes, J. Chem. Technol. Biotechnol. 94 (2019) 2738–2748.

[76] A. Ter Heijne, D. Liu, M. Sulonen, T. Sleutels, F. Fabregat-Santiago, Quantification of bio-anode capacitance in bioelectrochemical systems using Electrochemical Impedance Spectroscopy, J. Power Sources 400 (2018) 533–538.

[77] A. Deeke, T.H.J.A. Sleutels, T.F.W. Donkers, H.V.M. Hamelers, C.J.N. Buisman, A. ter Heijne, Fluidized capacitive bioanode as a novel reactor concept for the microbial fuel cell, Environ. Sci. Technol. 49 (2015) 1929–1935.

[78] A. Deeke, T.H.J.A. Sleutels, H.V.M. Hamelers, C.J.N. Buisman, Capacitive bioanodes enable renewable energy storage in microbial fuel cells, Environ. Sci. Technol. 46 (2012) 3554–3560.

[79] C. Borsje, T. Sleutels, M. Saakes, C.J.N. Buisman, A. Ter Heijne, The granular capacitive moving bed reactor for the scale up of bioanodes, J. Chem. Technol. Biotechnol. 94 (2019) 2738–2748.

[80] L. Caizán-Juanarena, C. Borsje, T. Sleutels, D. Yntema, C. Santoro, I. Ieropoulos, F. Soavi, A. ter Heijne, Combination of bioelectrochemical systems and electrochemical capacitors: principles, analysis and opportunities, Biotechnol. Adv. 39 (2020), 107456.

[81] C. Santoro, X.A. Walter, F. Soavi, J. Greenman, I. Ieropoulos, Self-stratified and self-powered micro-supercapacitor integrated into a microbial fuel cell operating in human urine, Electrochim. Acta 307 (2019) 241–252.

[82] C. Santoro, C. Flores-Cadengo, F. Soavi, M. Kodali, I. Merino-Jimenez, I. Gajda, J. Greenman, I. Ieropoulos, P. Atanassov, Ceramic Microbial Fuel Cells Stack: power generation in standard and supercapacitive mode, Sci. Rep. 8 (2018) 3281.

[83] C. Santoro, M. Kodali, N. Shamoon, A. Serov, F. Soavi, I. Merino-Jimenez, I. Gajda, J. Greenman, I. Ieropoulos, P. Atanassov, Increased power generation in supercapacitive microbial fuel cell stack using FeNC cathode catalyst, J. Power Sources 412 (2019) 416–424.

[84] I. Ieropoulos, J. Greenman, C. Melhuish, Urine utilisation by microbial fuel cells; energy fuel for the future, Phys. Chem. Chem. Phys. 14 (2012) 94–98.

[85] C. Santoro, M.J. Salar Garcia, X.A. Walter, J. You, P. Theodosiou, I. Gajda, O. Obata, J. Winfield, J. Greenman, I. Ieropoulos, Urine in bioelectrochemical systems: an overall review, ChemElectroChem 7 (2020) 1312–1331.

[86] S. Bouatra, F. Aziat, R. Mandal, A.C. Guo, M.R. Wilson, C. Knox, T.C. Bjorndahl, R. Krishnamurthy, F. Saleem, P. Liu, Z.T. Dame, J. Poelzer, J. Huynh, F.S. Yallou, N. Psychogios, E. Dong, R. Bogumil, C. Roehring, D.S. Wishart, The human urine metabolome, PloS One 8 (9) (2013), e73076.

[87] S.G. Barbosa, L. Peixoto, A. Ter Heijne, P. Kuntke, M.M. Alves, M.A. Pereira, Investigating bacterial community changes and organic substrate degradation in microbial fuel cells operating on real human urine, Environ. Sci.: Water Res. Technol. 3 (2017) 897–904.

[88] X.A. Walter, C. Santoro, J. Greenman, I. Ieropoulos, Self-stratifying microbial fuel cell: the importance of the cathode electrode immersion height, Int. J. Hydrogen Energy 44 (2019) 4524–4532.

[89] X.A. Walter, C. Santoro, J. Greenman, I.A. Ieropoulos, Scalability of self-stratifying microbial fuel cell: towards height miniaturisation, Bioelectrochemistry 127 (2019) 68–75.

[90] F. Poli, J. Seri, C. Santoro, F. Soavi, Boosting microbial fuel cells performance by the combination of an external supercapacitor: an electrochemical study, ChemElectroChem 7 (2020) 893–903.

[91] B.E. Logan, B. Hamelers, R. Rozendal, U. Schröder, J. Keller, S. Freguia, P. Aelterman, W. Verstraete, K. Rabaey, Microbial fuel cells: methodology and technology, Environ. Sci. Technol. 40 (2006) 5181–5192.

[92] R. Rossi, B.P. Cario, C. Santoro, W. Yang, P.E. Saikaly, B.E. Logan, Evaluation of electrode and solution area-based resistances enables quantitative comparisons of factors impacting microbial fuel cell performance, Environ. Sci. Technol. 53 (2019) 3977–3986.

[93] T. Cai, Y. Huang, M. Huang, Y. Xi, D. Pang, W. Zhang, Enhancing oxygen reduction reaction of supercapacitor microbial fuel cells with electrospun carbon nanofibers composite cathode, Chem. Eng. J. 371 (2019) 544–553.

[94] R. Rossi, W. Yang, E. Zikmund, D. Pant, B.E. Logan, In situ biofilm removal from air cathodes in microbial fuel cells treating domestic wastewater, Bioresour. Technol. 265 (2018) 200–206.

[95] M. Santini, S. Marzorati, S. Fest-Santini, S. Trasatti, P. Cristiani, Carbonate scale deactivating the biocathode in a microbial fuel cell, J. Power Sources 356 (2017) 400–407.

[96] M. Santini, M. Guilizzoni, M. Lorenzi, P. Atanassov, E. Marsili, S. Fest-Santini, P. Cristiani, C. Santoro, Three-dimensional X-ray microcomputed tomography of carbonates and biofilm on operated cathode in single chamber microbial fuel cell, Biointerphases 10 (2015), 031009.

[97] B.E. Logan, M.J. Wallack, K.Y. Kim, W. He, Y. Feng, P.E. Saikaly, Assessment of microbial fuel cell configurations and power densities, Environ. Sci. Technol. Lett. 2 (2015) 206–214.

[98] Z. Ge, J. Li, L. Xiao, Y. Tong, Z. He, Recovery of electrical energy in microbial fuel cells: brief review, Environ. Sci. Technol. Lett. 1 (2013) 137–141.